

AD _____

Award Number: DAMD17-02-1-0097

TITLE: Prostate Carcinoma Detection using Combined Ultrasound, Elasticity and Tissue Strain-Hardening Imaging

PRINCIPAL INVESTIGATOR: Stanislav Emelianov, Ph.D.

CONTRACTING ORGANIZATION: The University of Texas at Austin
Austin, TX 78712

REPORT DATE: January 2006

TYPE OF REPORT: Annual

PREPARED FOR: U.S. Army Medical Research and Materiel Command
Fort Detrick, Maryland 21702-5012

DISTRIBUTION STATEMENT: Approved for Public Release;
Distribution Unlimited

The views, opinions and/or findings contained in this report are those of the author(s) and should not be construed as an official Department of the Army position, policy or decision unless so designated by other documentation.

20060606095

REPORT DOCUMENTATION PAGE				Form Approved OMB No. 0704-0188	
<small>Public reporting burden for this collection of information is estimated to average 1 hour per response, including the time for reviewing instructions, searching existing data sources, gathering and maintaining the data needed, and completing and reviewing this collection of information. Send comments regarding this burden estimate or any other aspect of this collection of information, including suggestions for reducing this burden to Department of Defense, Washington Headquarters Services, Directorate for Information Operations and Reports (0704-0188), 1215 Jefferson Davis Highway, Suite 1204, Arlington, VA 22202-4302. Respondents should be aware that notwithstanding any other provision of law, no person shall be subject to any penalty for failing to comply with a collection of information if it does not display a currently valid OMB control number. PLEASE DO NOT RETURN YOUR FORM TO THE ABOVE ADDRESS.</small>					
1. REPORT DATE (DD-MM-YYYY) 01-01-2006		2. REPORT TYPE Annual		3. DATES COVERED (From - To) 31 Dec 04 - 30 Dec 05	
4. TITLE AND SUBTITLE Prostate Carcinoma Detection using Combined Ultrasound, Elasticity and Tissue Strain-Hardening Imaging				5a. CONTRACT NUMBER	
				5b. GRANT NUMBER DAMD17-02-1-0097	
				5c. PROGRAM ELEMENT NUMBER	
6. AUTHOR(S) Stanislav Emelianov, Ph.D. E-Mail: emelian@mail.utexas.edu				5d. PROJECT NUMBER	
				5e. TASK NUMBER	
				5f. WORK UNIT NUMBER	
7. PERFORMING ORGANIZATION NAME(S) AND ADDRESS(ES) The University of Texas at Austin Austin, TX 78712				8. PERFORMING ORGANIZATION REPORT NUMBER	
9. SPONSORING / MONITORING AGENCY NAME(S) AND ADDRESS(ES) U.S. Army Medical Research and Materiel Command Fort Detrick, Maryland 21702-5012				10. SPONSOR/MONITOR'S ACRONYM(S)	
				11. SPONSOR/MONITOR'S REPORT NUMBER(S)	
12. DISTRIBUTION / AVAILABILITY STATEMENT Approved for Public Release; Distribution Unlimited					
13. SUPPLEMENTARY NOTES					
14. ABSTRACT: <p>The underlying hypothesis of our study is that remote, non-invasive measurements of prostate elasticity are possible and may increase the detection and/or characterization of potentially malignant masses in the prostate. The purpose of this study is to develop ultrasound technology to produce high-resolution strain images of the prostate for remote evaluation of the strain dependent elastic (Young's or shear) modulus. The main objective of our research program is to test the hypothesis that quantitative elasticity images of the prostate can be obtained using real-time ultrasound and manual deformation of the gland. To achieve this objective, we have developed speckle tracking algorithms and methods for strain and elasticity imaging of prostate. The developed imaging methods were tested using tissue-mimicking phantoms. Next, we will conduct experimental studies using tissue-containing phantoms, and well-defined clinical studies. At the conclusion of the study, a prototype of clinical imaging system will be designed.</p>					
15. SUBJECT TERMS Prostate Carcinoma, Medical Imaging, Ultrasound, Elasticity					
16. SECURITY CLASSIFICATION OF:			17. LIMITATION OF ABSTRACT	18. NUMBER OF PAGES	19a. NAME OF RESPONSIBLE PERSON
a. REPORT U	b. ABSTRACT U	c. THIS PAGE U			USAMRMC
			UU	16	19b. TELEPHONE NUMBER (include area code)

Table of Contents

Cover.....	
SF 298.....	2
Table of Contents.....	3
Introduction.....	4
Body.....	5
Key Research Accomplishments.....	13
Reportable Outcomes.....	13
Conclusions.....	14
References.....	14
Appendices.....	16

INTRODUCTION:

Prostate cancer is the most common cancer in American men, and is the second leading cause of cancer death in men, exceeded only by lung cancer. Among men diagnosed with prostate cancer, 85% of all prostate cancers are found while they are still localized (that is, confined to the prostate), and the 5-year relative survival rate for men with localized prostate cancer is 100%. Thus, there presently is a definite and urgent clinical need for a technique that is widely available, is simple to perform, is safe, and that can detect and adequately diagnose prostate cancer.

The American Cancer Society estimates that during 2004, approximately 220,000 new cases of prostate cancer will be diagnosed, and approximately 30,000 men will die of this disease in the United States.¹ Therefore, an increasing emphasis must be made on early detection and screening with advanced imaging techniques and prostate specific antigen (PSA) test as initial indicator.^{2,3} PSA alone yields significant number (30 - 40%) of false-positive results and (20-30%) of false negative results.⁴ The ultrasound-guided biopsy and even biopsy under transrectal MRI are not free of limitations.⁵⁻⁷ Tumor staging is especially difficult due to limited contrast between cancerous and normal tissues. Thus, biopsy could be performed more accurately under the guidance of real-time imaging with enhanced tissue contrast, resolution and specificity to malignant tumors.^{3,8,9}

Digital rectal examination (DRE), a traditional method of evaluating the prostate gland, is a mainstay for detecting prostate cancer. The DRE is widely used by primary care physicians and medical specialists to identify patients needing a prostate biopsy. Although the prostate gland is readily accessible to digital examination, DRE is very inaccurate. The DRE effectiveness is limited by its subjective nature and its ability to palpate only the posterior portion of the gland.^{10,11}

Prostate specific antigen, the most important of all tumor markers, is currently used for early detection of prostate cancer.⁴ The PSA level of more than 4 ng/ml indicates possible prostate cancer. However, PSA test alone is not sufficient for cancer diagnosis, yielding about 40% false-positive results. Even ten-fold increase of PSA level to 40 ng/ml does not guarantee the presence of malignant tumor.⁴

Diagnostic imaging of the prostate with currently available imaging techniques is similarly problematic. Medical imaging systems such as CT, MRI, and ultrasound, are widely used for the early detection of cancer. However, despite the great and ongoing progress in medical imaging, it is recognized that only a small percentage of tumors can be diagnosed through noninvasive screening. Indeed, none of the existing imaging modalities alone can reliably detect and differentiate cancerous tissue. For example, transrectal ultrasonography (TRUS) has emerged as the most common imaging modality for prostate diagnosis.¹² However, both the sensitivity and specificity of transrectal ultrasound remain too low for a reliable screening test. Reports have compared DRE to transrectal ultrasonography (TRUS) and measurement of serum prostate-specific antigen concentration.¹³ Most studies have concluded that DRE is useful in detecting prostate cancer and should be used in combination with PSA and TRUS for early prostate cancer detection.^{1,13} TRUS is the most widely used imaging technique for non-invasive assessment of prostatic gland and, prostate volume as well as guiding biopsy procedures. On the other hand, ultrasound guidance helps physician to visualize the extent of prostate gland, not the extent of malignant tumors if present. Therefore, biopsy performed by random sampling may yield significant number of false-negative results.^{14,15}

The fundamental goal of our research program is to develop an advanced imaging technology – grayscale ultrasound combined with elasticity and strain hardening imaging – capable of more accurate and earlier detection and diagnosis of prostate pathology, sequential monitoring of cancer treatment, and superior targeting and guidance of tissue biopsy.

BODY:

Administrative note: The results presented here is a concise summary of the work conducted in the past 12 months. Indeed, even though the grant was awarded in 2002, both Principal Investigator of this project, Dr. Emelianov, and Co-Investigator, Dr. Aglyamov, moved to the University of Texas at Austin during summer of 2002, and it took nearly 2 years to transfer the award to the new institution. Therefore, this reports effectively covers initial stage of the project, i.e., months 1-12 of the statement of work.

Per the statement of work of the proposal, there are the following research areas in developing combined ultrasound, elasticity and tissue strain-hardening imaging of prostate.

Design and build prostate mimicking phantoms.

To develop and improve ultrasound elasticity imaging technique, it is necessary to produce phantoms which can reliably mimic the properties of human tissue. Before these phantoms can be produced, however, it is also necessary to investigate and to be able to precisely manipulate the properties of the phantom materials. In addition, the properties of the materials must be stable over time, and the phantoms should be easy to produce and have a long shelf-life.

Based on our own measurements and the literature data,^{16,17} the material for adequate manufacturing of mechanical models of prostate should cover the range of Young's modulus from 1 to 300 kPa (Fig. 1). In addition, a compatible material with Young's modulus on the order of 1 MPa is needed to simulate the surrounding internal tissue including rectum wall.

In ultrasound elasticity imaging, the most notable properties of the phantom material are the acoustic and mechanical characteristics. There are several gel- and rubber-based materials that can be used to produce tissue phantoms.

In our investigation, we focused our attention on poly(vinyl alcohol) (PVA) hydrogels because of several unique properties of this material.¹⁸⁻²¹ First, a rich set of parameters (molecular weight and concentration of PVA, number of freeze/thaw cycles, concentration of crosslinking additives, etc.) allows producing hydrated gels of high water content and variable elasticity (Young's modulus). Second, the fabricated hydrogels are easy to produce, nontoxic, stable, durable and have a reasonable shelf-life. Finally, PVA hydrogels can be used in multi-modality studies using optical, X-ray, ultrasound and NMR (MRI) imaging techniques.

Therefore, poly(vinyl) alcohol was used to produce tissue mimicking hydrogel phantoms. PVA crystalline granules were obtained from Celanese Chemicals (Celvol 165). These granules were first mixed with water to obtain a desired weight percentage solution. The solution was then heated to approximately 95°C to achieve complete dissolution. The solution next underwent a period of degassing to remove any residual dissolved gases that were introduced during dissolution of the PVA granules. At this point silica gel particles were added to the PVA solutions to increase the acoustic scattering of the resulting hydrogels. PVA solutions were then cast into desired molds and processed through repeated freeze/thaw cycles to induce crosslinking of the polymer. Each freeze/thaw cycle consisted of 17 hours at -3 °C, followed by 7 hours at 23 °C. To mimic various structures of different elasticity, PVA solutions of 4%, 7%,

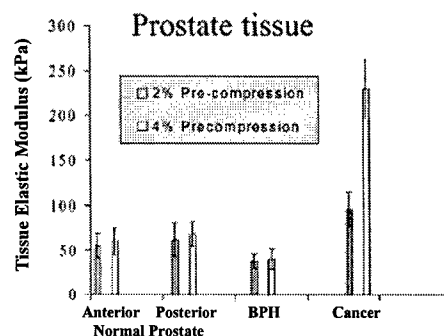


Fig. 1: Mechanical properties of prostate under different precompressions.¹⁶

and 10% were used (Fig. 2). While not undergoing freeze/thaw cycles, PVA samples were stored submerged in clean water at room temperature.

To assess the mechanical properties of the material, the PVA solutions were cast into cylindrical molds measuring 34 mm in diameter and 18 mm in height. The Young's modulus of each sample was measured with compression tests using an Instron tester (In-Spec 2200) with a 125 N load cell and 50 mm diameter plates. Force-deformation curves were collected for each sample including 0% to ~20% deformation of each sample at a deformation rate of 0.2 mm/s. The area and initial length of the samples were used to then produce a stress versus strain curve for each sample, and a linear regression was run on each sample between approximately 1% and 5% deformation to calculate the Young's modulus (Fig. 2).

The attenuation and the speed of sound in PVA hydrogels was measured to be 0.2 dB/cm/MHz (or less) and 1530 m/s, respectively, and did not change appreciably with freeze/thaw cycles or PVA concentration. The mechanical strength of hydrogels was shown to increase proportional to the PVA concentration (Fig. 2 and Table I below).

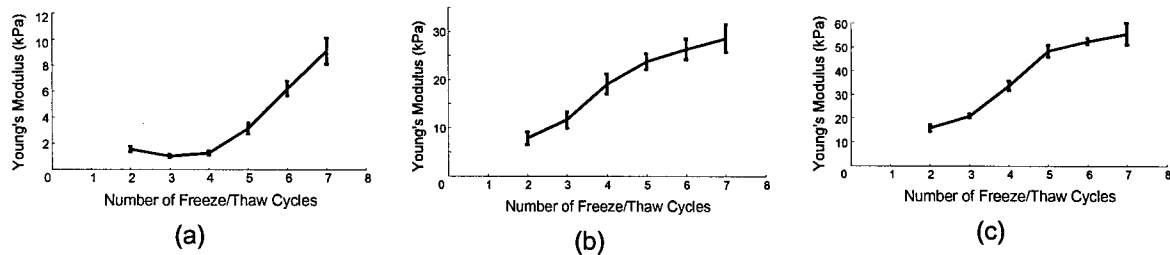


Fig. 2: Young's modulus changes with number of freeze/thaw cycles for a) 4% PVA solution, b) 7% PVA solution, and c) 10% PVA solution. The demonstrated nearly twenty fold dynamic range of elasticity is appropriate to mimic prostate and various prostate pathologies.

Increasing the number of freeze/thaw cycles increases nonlinearly the mechanical strength of PVA hydrogels (Fig. 2).²¹ The PVA gels maintained their size, shape, and acoustic and mechanical properties when stored in water at room temperature (Fig. 3).

Number of Cycles	Young's modulus		
	4% PVA	7% PVA	10% PVA
2	1.5 ± 0.2	7.8 ± 1.3	15.8 ± 1.4
3	1.0 ± 0.1	11.6 ± 1.7	20.9 ± 0.8
4	1.2 ± 0.2	19.1 ± 2.1	33.6 ± 2.0
5	3.3 ± 0.4	23.8 ± 1.3	48.2 ± 2.4
6	6.2 ± 0.5	26.4 ± 2.2	52.3 ± 1.3
7	9.1 ± 1.0	28.6 ± 2.9	55.5 ± 4.3

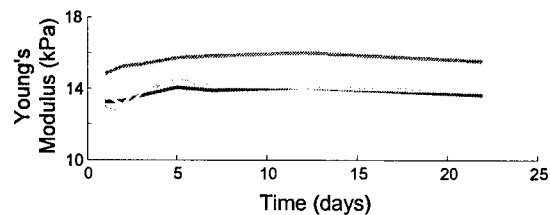


Fig. 3: Time stability of PVA samples

In transrectal ultrasound examination of the prostate (Fig. 4a), two types of probes are commonly used – the side-fire scanhead (i.e., the array of transducers is positioned on a side of the probe) and the end-fire scanhead (i.e., the array of transducers is positioned on the end of the probe). The probes and corresponding imaging planes are presented in Fig. 4b. Therefore, we have produced phantoms to account for two types of ultrasound prostate probes available. The probes determine not only the imaging plane but also the way the imaging study is performed (Fig. 4a) and how the deformations required for elasticity imaging can be applied.

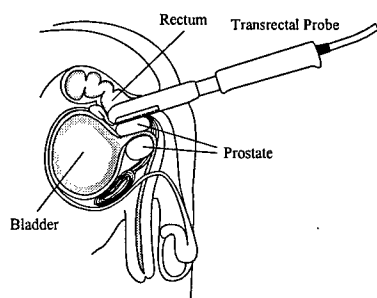


Fig. 4a: Transrectal ultrasound imaging of the prostate (side-fire probe is shown).

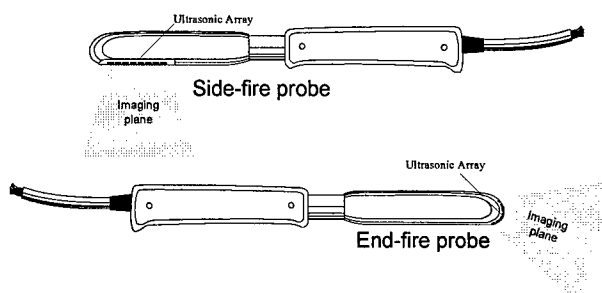


Fig. 4b: Schematic view of side-fire (top) and end-fire (bottom) transrectal probe for combined ultrasound, elasticity and strain-hardening imaging.

Prostate phantoms were produced using PVA solutions of various concentrations undergoing different number of freeze/thaw cycles. In our initial studies, the background prostate tissue was made first by preparing a cylindrical piece of PVA (7% concentration) with two cylindrical voids – one to simulate the urethra and the other one to simulate the cancerous lesion (Fig. 5a). The voids were then filled with different concentrations of PVA, and the overall cylinder was cast into a rectangular mold (Fig. 5b). The inclusion was produced using 10% PVA. To provide acoustic backscattered signal and visual contrast, 2% silica gel particles and graphite flakes were added into solution, correspondingly. The background for the prostate was produced using 7% PVA containing 2% silica gel particles. The overall phantom, therefore, consists of stiff rectal wall (top layer in Fig. 5b), prostate with soft urethra and hard lesion, and the background tissue. These phantoms closely mimic the cross-sectional geometry, acoustic properties and elasticity contrast of prostate and cancerous lesion. These phantoms can be used with either side-fire or end-fire types of the ultrasound probes presented in Fig. 4.

Finally, we have also produced a rubber based phantom to be used exclusively with end-fire ultrasound imaging probe. This rubber-made phantom contains prostate with 2 lesions inside – one hard and one soft lesion (Fig. 6).

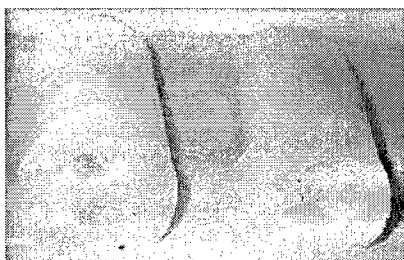


Fig. 5a: PVA-based samples mimicking prostate with urethra and lesion.

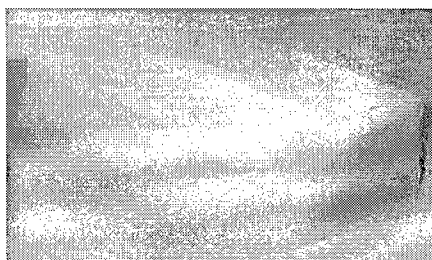


Fig. 5b: Phantom to mimic rectal wall, background tissue and prostate gland with lesion.

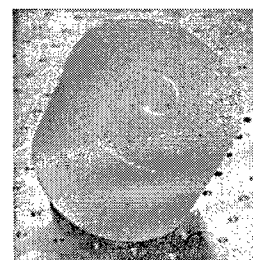


Fig. 6: Prostate phantom to be used with an end-fire probe.

The representative ultrasound images of the phantoms similar to one presented in Fig. 5 are demonstrated in Fig. 7. In these side-fire images the prostate is shown as a round object in the middle. The transducer is positioned on the top and it is in contact with a rectal wall – a layer of tissue above the prostate. The background tissue has weaker backscattered signal as it is often observed in clinical images. The urethra can be hypoechoic and indistinguishable from the prostate tissue. Finally, the cancerous lesion or lesions can be either hyperechoic or hypoechoic or invisible in ultrasound images – again, our phantoms can clearly simulate all of these cases.

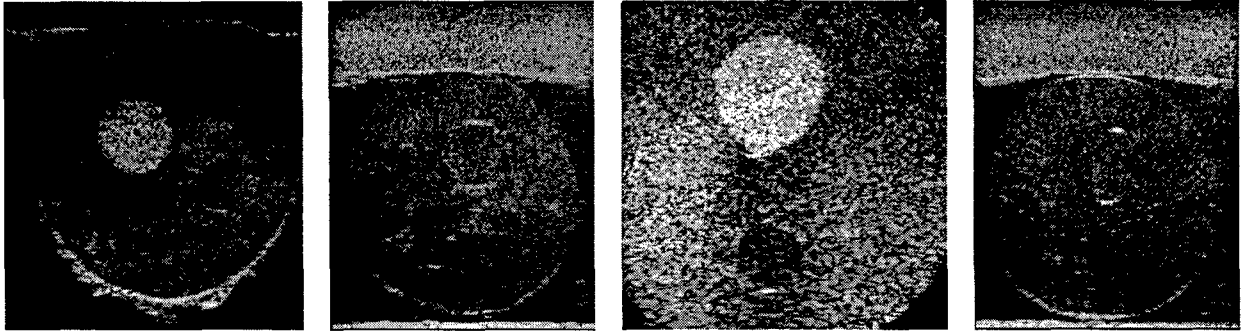


Fig. 7: Representative ultrasound images of the prostate mimicking phantom.

The results presented above demonstrate that poly(vinyl alcohol) can be used to produce complex tissue mimicking phantoms with desired acoustic and mechanical properties. The number of freezing and thawing cycles and concentration of aqueous solution of different molecular weight PVA can be manipulated to control properties such as the overall water content and mechanical strength while acoustic properties remain nearly the same. Using PVA, time stable and sturdy composite phantoms with distinct mechanical structures well adhered to each other were produced.

Design and construct the deformation system and provide all necessary modifications of the deformational system as determined from the studies.

Internal deformations, needed for elasticity imaging, can be created within the prostate either using carefully controlled, motion-axis assisted device to which the ultrasound probe is attached, or using free-hand surface deformations produced by the manual motion of the imaging probe itself. We have pursued both directions to ultimately compare the performance of any developed displacement, strain and elasticity imaging techniques.

However, from clinical stand point, the free-hand deformations are desired since this approach will not require any specialized equipment to perform the examination. Indeed, during a short, continuous deformation producing no more patient discomfort than standard DRE test, real-time ultrasound can capture information needed for elasticity imaging. Based on current clinical criteria, transrectal ultrasound is already widely used for prostate diagnosis and patients will not be subjected to any significant additional examination time to perform elasticity imaging of the prostate.

Therefore, the focus of our study was and will remain in developing a free-hand elasticity imaging techniques where no additional devices will be required. In addition, elasticity imaging part of the system does not require any specific modifications of the transrectal probe. Indeed, only signal and image processing of ultrasound frames is required to image elasticity of tissue.

Develop and/or modify existing algorithms for ultrasound speckle tracking, strain imaging and adaptive elasticity mapping needed for prostate elasticity imaging.

Ultrasound elasticity imaging consists of three main components: a) application of surface deformation to the study object;^{22,23} b) multi-dimensional speckle tracking and evaluation of internal tissue motion, i.e., measurement of displacement and strain components;²³⁻²⁵ and c) reconstruction of the spatial distribution of elastic modulus in the imaging plane.²⁶⁻²⁹ The goal of elasticity imaging is to reconstruct maps of Young's modulus using available estimates of displacement and strain components.³⁰

Speckle tracking is based on time-delay estimation. There are numerous speckle tracking techniques that are based on the estimation of the maximum (minimum) of a pattern matching function. The commonly used pattern matching functions are sum of absolute differences, sum of squared differences, normalized cross-correlation and non-normalized cross-correlation. Usually, the algorithms based on sum absolute differences and sum squared differences have a low computational cost and a low quality of the displacements estimation in comparison with cross-correlation algorithms.

We have developed several speckle tracking algorithms and methods for displacement and strain estimation. Specifically, we have investigated time-delay algorithms based on 1) sum of absolute differences (SAD), 2) sum of squared differences (SSD), 3) spline-based representation of the signal, 4) cross-correlation. Each technique can generally provide an estimation of integer displacement, i.e., displacement value rounded to a nearest differential position of a pixel. To find sub-integer displacement, i.e., precise position of the maximum or minimum of the corresponding time-delay estimation function, we investigated several interpolation techniques such as 1) 3-point parabolic interpolation, 2) spline interpolation, 3) phase zero crossing. The computational efficiency of each technique was analyzed and compared.

Furthermore, we performed numerical simulations to compare the performance of the developed algorithms. The results of the study are presented in Table II and Fig. 8. Here the ideal deformation (i.e., one-dimensional motion along the ultrasound beam) of various magnitude (0-4% strain) was modeled, and corresponding ultrasound frames were generated assuming 7.5 MHz, 60% fractional bandwidth transducer. The ultrasound signal was sampled at 40 MHz. The motion tracking algorithms were applied to simulated ultrasound data to compute both axial displacement and axial strain. The measured displacement and strain were then compared to the prescribed values, and signal-to-noise ratios (SNRs) were estimated.

For the uniform motion of the sample (i.e., where the entire sample moves as a whole and there are no differential displacement within the sample), the displacement SNRs are compared in the Table II. Clearly, the spline-interpolated SSD approach outperforms all of the other techniques except somewhat comparable cross-correlation based speckle tracking technique. All other techniques demonstrate significantly lower performance.

Table II	Time-delay method	SAD	SSD	SSD	Correlation	Correlation	Correlation
	Interpolation method	Parabolic	Parabolic	Spline	Parabolic	Spline	Zero crossing
	Displacement SNR	33.8	105.5	2516.0	112.5	134.7	1676.0

However, the performance of each technique changes dramatically with deformations of the sample. Indeed, the displacement SNR drops below 70, and it is also strain dependent (Fig. 8a). As indicated in this figure, correlation based techniques have most stable performance which does not change appreciably with applied deformations. However, for applied deformation of 2% and more, the SSD/SAD techniques are exhibiting similar performance, and large deformations the parabolic interpolation SAD method outperforms all other techniques. Similar trend is observed for strain SNR – the SSD/SAD methods are not desired for measurements of low deformations while correlation techniques are stable over large ranges of applied strain. Again, parabolic interpolation SAD is a better choice for large (> 2 %) strains. Note that these results were obtained under simplified conditions (i.e., one-dimensional motion, etc.) and should be considered as guidance only.

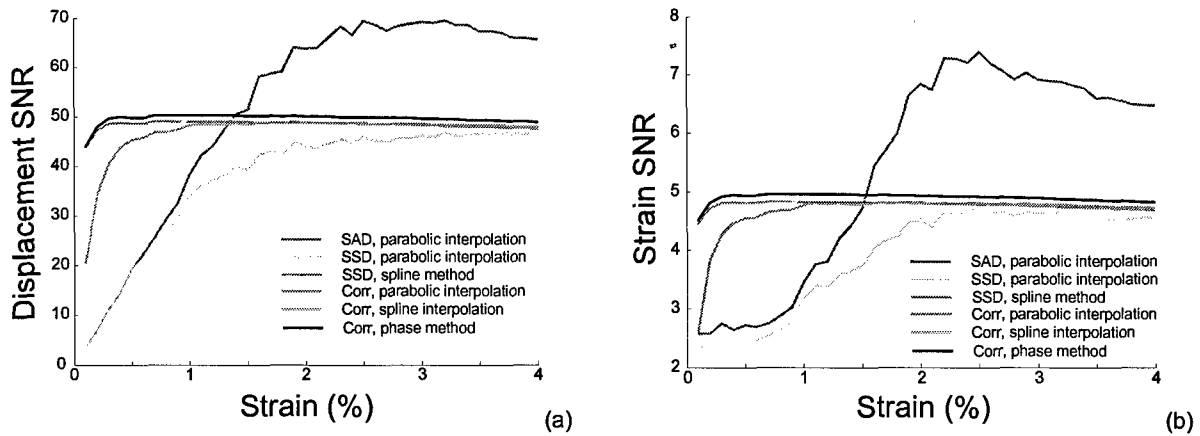


Fig. 8: Displacement and strain signal-to-noise ratios contrasted for various speckle tracking algorithms.

Test initially the performance of prostate elasticity imaging using prostate phantoms.

We have initially evaluated the performance of speckle tracking techniques using prostate phantoms. The results reported here were obtained from a phantom with two lesions – one lesion was approximately 2 times harder than the prostate tissue, and the other lesion has the same stiffness compared to the elasticity of the gland. The initial state of the prostate and prostate after 2% deformation is depicted in ultrasound images in Fig. 9a and Fig. 9b, correspondingly. The ultrasound array transducer, operating at 5 MHz, was positioned in contact with modeled rectum wall to deform the wall and adjacent tissue including the prostate gland, where deformations were continuously imaged with ultrasound, and captured for off-line elasticity processing. Deformations were produced directly with the ultrasound probe. As the probe is gently pushed against the rectal wall (similar to palpation or DRE examination), controlled deformations were applied resulting in controlled deformation of the prostate and surrounding tissue.

During deformation, many consecutive ultrasound frames were captured and stored for off-line data processing. The frame-to-frame displacement and strain images were computed using correlation based algorithm described in detail elsewhere.^{25,31,32} The strain image is presented in Fig. 9c where the distribution of normal axial strain is displayed using a quantitative color map. Smaller strain magnitudes (dark regions) signal harder material, and vice versa. In this image the harder lesion can be clearly identified. The second lesion, as expected, is not detected in strain image since it has no mechanical contrast with the background tissue. The boundaries of the prostate are also highlighted due to overall difference between the prostate and surrounding tissue.

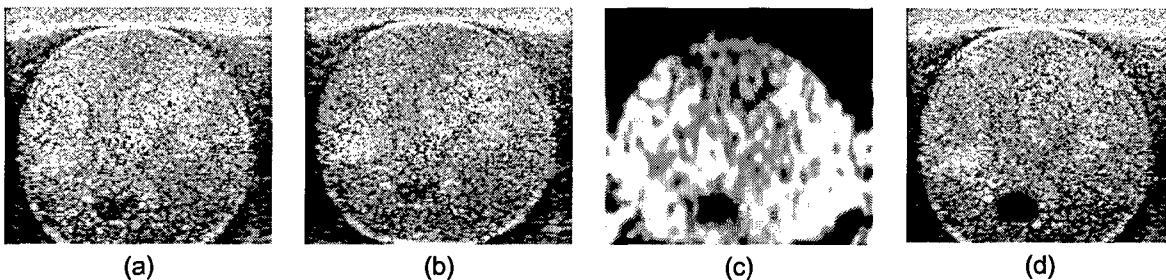


Fig. 9: Ultrasound image of the prostate with two lesions a) before and b) after deformation applied with the ultrasound imaging probe. c) Strain image of the prostate initially identifying the harder lesion. d) Elasticity image overlaid on top of the ultrasound image indicating the prostate cancer.

To portray the lesion within the structural content, the ultrasound and elasticity images are combined in Fig. 9d. Here the elasticity image is overlaid on ultrasound image, i.e., ultrasound signal is displayed if elasticity of the region is smaller than the user-defined threshold, and vice versa. This image, again, clearly identifies the harder, cancerous lesion.

Develop and produce sophisticated and more realistic phantoms of the prostate.

We have developed more sophisticated phantoms of prostate based on the technology described earlier. To evaluate the performance of each individual component of the ultrasound and elasticity imaging system, we designed phantoms with emphasis to a specific property. For example, to evaluate spatial resolution of the elasticity imaging, phantom with inclusions of different sizes are needed. The top choice of the phantom material for this study is poly (vinyl alcohol). This material can be molder into desired shape by simply undergoing the freezing and de-freezing cycle(s). Such cross-linking of the PVA does not change ultrasonic properties of gel while increasing mechanical strength of the phantom. In addition, additives can be used to produce optically transparent gels.

Our phantoms closely resemble the commercially available ultrasound phantoms such as one presented in Fig. 10a. These phantoms closely resemble both geometrical and mechanical properties of the prostate and surrounding tissue, and may have several lesions position throughout the prostate. We have developed the technique and procedure to manufacture sophisticated phantoms with tumors of various shapes, sizes and mechanical/ultrasound contrast positioned at different locations within the phantom. Generally, elasticity imaging is sensitive to less than 50% change of tissue elasticity³³ while most tumors are at least 2-3 times harder than the background tissue.^{30,34,35} The spatial resolution of elasticity imaging is frequency dependent,³⁶ and for 5-7 MHz range the spatial resolution³³ is about 1 mm.

One of the phantom designs is presented in Fig. 10b and Fig. 10c where 52-mm prostate with two lesions is was produced first. Both lesions have acoustic contrast and can be easily detected by ultrasound imaging, however, only one lesion has elastic contrast. The prostate is then embedded into a rectangular (12 by 7 by 10 cm³) container (Fig. 10c) filled with homogeneous material. Another sophisticated tissue equivalent ultrasound prostate phantom (similar to CIRS phantom in Fig. 10a) was developed to mimic the prostate, along with structures simulating the rectal wall, seminal vesicles, and urethra. Both phantoms are constructed such that both types of ultrasound prostate probes (Fig. 4b) can be used to image the phantom. In comparison, CIRC phantom s can only be used with side-fire ultrasound probes.

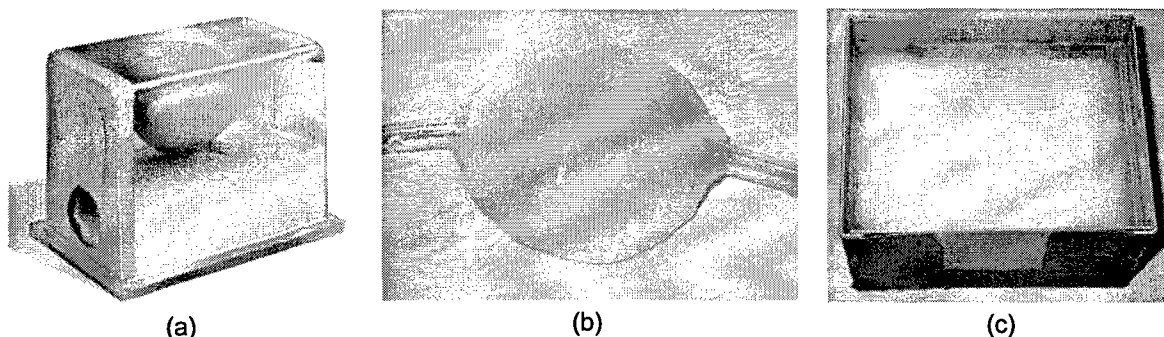


Fig. 10: a) Commercially available prostate phantoms. b) Prostate gland with urethra c) embedded into otherwise homogeneous phantom with thin layer of harder material to simulate rectal wall.

Investigate thoroughly the speckle tracking algorithms and strain imaging methods for prostate elasticity imaging.

Elasticity reconstruction algorithms are highly dependent on the signal-to-noise ratio (SNR) of the input data, i.e., displacement and strain SNR. The higher strain SNR used, the higher contrast-to-noise ratio is possible in elasticity imaging. Based on the overall needs of prostate elasticity imaging, including elasticity visualization, strategies for optimal displacement and strain imaging were studied.

Using the ultrasound frames captured during surface applied deformation of the prostate phantom, we have investigated the displacement and strain SNRs. Compared to results presented before (Fig. 8), the displacement SNR is optimal at 1 % of applied strain, and there is no significant difference between various speckle tracking techniques for higher strains. For lower strains, correlation-based and spline-based techniques are generally outperforming the SSD/SAD counterparts. The measurements performed at 1-2% applied strain have better SNR. Interestingly, all methods demonstrate uniform performance at 2.0-2.5% applied deformation.

The results presented in Fig. 11 can be explained by the 3-D motion and deformation of the phantom (compared to 1-D motion/deformation in simulated study). It is known that strain decorrelation is a dominant source of error in strain imaging. However, it was not expected that most methods would behave similarly after some strain threshold. This result has direct implication of real-time implementation of strain imaging – the computationally effective SAD or SSD with parabolic interpolation will be used in hardware implementation of strain imaging. Indeed, SAD/SSD is about 10 times more efficient compared to cross-correlation methods.

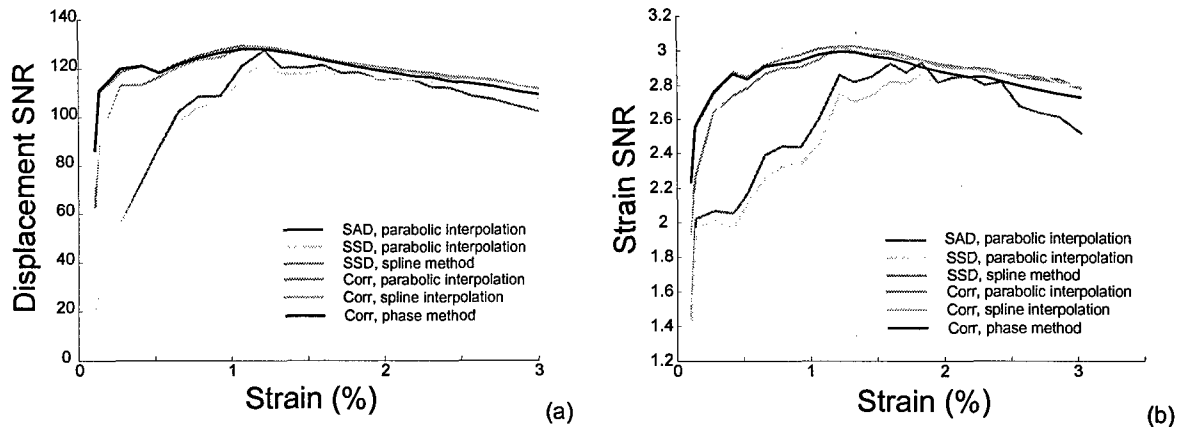


Fig. 11: Displacement and strain signal-to-noise ratios contrasted for various speckle tracking algorithms. The results were obtained from prostate phantom using 5 MHZ prostate probe.

The strain SNR is further tabulated in Table III below. Here SNR values for different applied strains (0.15%, 0.5%, and 0.8%) are presented for quantitative comparison. Clearly, phase-based correlation technique and spline-based SSD have higher SNR values.

Time-delay method	SAD	SSD	SSD	Correlation	Correlation	Correlation
Interpolation method	Parabolic	Parabolic	Spline	Parabolic	Spline	Zero crossing
Strain SNR @ 0.15%	2.02	1.96	2.55	2.26	2.16	2.56
Strain SNR @ 0.5%	2.02	1.96	2.85	2.79	2.93	2.83
Strain SNR @ 0.8%	2.44	2.33	2.95	2.90	3.02	2.92

KEY RESEARCH ACCOMPLISHMENTS:

- Identified several tissue-mimicking materials and investigated the acoustic and mechanical properties of poly(vinyl) alcohol to demonstrate the appropriateness of PVA for manufacturing of prostate phantoms
- Designed and built PVA-based prostate mimicking phantoms with desired mechanical and ultrasound properties of normal prostate and prostate abnormalities.
- Developed several ultrasound speckle tracking algorithms for displacement estimation, strain imaging and elasticity mapping needed for prostate elasticity imaging.
- Initially tested the performance of prostate elasticity imaging using tissue-mimicking phantoms.
- Compared the developed algorithms for specific needs of prostate elasticity imaging (i.e., the geometry of the probe, prostate and surrounding tissue, imaging plane and scan format, and nature of externally produced deformations) and quantified the performance of each technique.
- Designed and built several sophisticated prostate phantoms with structures simulating prostate (normal and with pathologies), the rectal wall, seminal vesicles, and urethra.

REPORTABLE OUTCOMES:

- S.Y. Emelianov, M.F. Hamilton, Yu.A. Ilinskii, and E.A. Zabolotskaya, "Nonlinear dynamics of a gas bubble in an incompressible elastic medium," *Journal of the Acoustical Society of America*, 115, pp. 581-588 (2004)
- X. Chen, M.J. Zohdy, S.Y. Emelianov, and M. O'Donnell, "Lateral speckle tracking using synthetic lateral phase," *IEEE Transactions on Ultrasonics, Ferroelectrics, and Frequency Control*, 51(5), pp. 540-550 (2004).
- S.Y. Emelianov, S.R. Aglyamov, J. Shah, S. Sethuraman, W.G. Scott, R. Schmitt, M. Motamedi, A. Karpouk, A. Oraevsky, "Combined ultrasound, optoacoustic and elasticity imaging," *Proceedings of the 2004 SPIE Photonics West Symposium*, vol. 5320, p. 101-112, (2004).
- S.Y. Emelianov, S.R. Aglyamov, J. Shah, S. Sethuraman, W.G. Scott, R. Schmitt, M. Motamedi, A. Karpouk, A. Oraevsky, "Synergy of ultrasound, elasticity, and optoacoustic imaging for improved detection and differentiation of cancerous tissue," *Abstracts of 147th Meeting of Acoustical Society of America*, May 24-28, *The Journal of the Acoustical Society of America*, 115(5), pt 2 of 2, pp.2411 (2004).
- R. Schmitt, G. Scott, S.Y. Emelianov, and R. Irving, "Development of high bandwidth transducers using injection molded 1-3 low pitch composites: a numerical study" *Proceedings of the Third International Conference on the Ultrasonic Measurement and Imaging of Tissue Elasticity*, p. 77 (2004)
- A.R. Skovoroda, D.D. Steele, T.L. Chenevert, M. O'Donnell and S.Y. Emelianov, "Three-dimensional static reconstructive elasticity imaging," submitted for publication (2005)
- J. Beck, S. Sethuraman, S. Mallidi, A. Karpouk, S.R. Aglyamov, and S.Y. Emelianov, "Tissue mimicking materials and phantoms for elasticity imaging," *Proceedings of the Fourth International Conference on the Ultrasonic Measurement and Imaging of Tissue Elasticity*, p. 107 (2005)

CONCLUSIONS:

The results presented here suggest that the combined ultrasound and elasticity imaging approach is possible and feasible. Since mechanical properties of the prostate are expected to change significantly with malignant lesions, and to a lesser extent with other types of lesions, it is anticipated that our imaging technology may detect and differentiate prostate pathology earlier than transrectal ultrasound (TRUS) examination alone or measurements of serum prostate-specific antigen (PSA) concentration. Ultrasonic access is very good since the prostate is typically located close to the rectum wall. High frequency, and hence high spatial resolution, ultrasound imaging is possible in most cases. Internal deformations, needed for elasticity imaging, can be created within the prostate using free-hand surface deformations produced by the imaging probe itself. Based on current clinical criteria, transrectal ultrasound is already widely used for prostate diagnosis as well as laboratory measurements, and therefore, all necessary pre-requisites for combined ultrasound and elasticity imaging of the prostate are readily available. Elasticity imaging could be integrated with an ultrasound imaging system requiring minimal or no changes in examination procedure and time. Patients will not be subjected to any additional time to perform combined imaging of the prostate. Finally, an urgent need exists for a more sensitive, specific, and earlier marker of prostate cancer – combined ultrasound, elasticity and strain hardening imaging technique may fill that need and become an important clinical tool of sufficient sensitivity and specificity for early diagnosis and improved therapy of prostate cancer.

REFERENCES:

1. Cancer Facts and Figures 2004. *American Cancer Society*. 2004.
2. Greenlee RT, Hill MB, Murray T, Thun M. Cancer Statistics 2001. *CA Cancer J. Clin.* 2001;51:15-36.
3. Eschenbach ACv. The challenge of prostate cancer. *CA Cancer J. Clin.* 1999;49:262-263.
4. Brawer MK. Prostate-specific antigen: Current status. *CA Cancer J. Clin.* 1999; 49:264-281.
5. Ikonen S, Karkkainen P, Kivisaari L, Salo JO, Taari K, Vehmas T, Tervahartiala P, Rannikko S. Magnetic resonance imaging of prostatic cancer: does detection vary between high and low Gleason score tumors? *Prostate*. 2000;43:43-48.
6. Benson MC, Whang IS, Pantuck A, et al. PSAD Means of distinguishing BPH and PC. *Journal of Urology*. 1992;147.
7. Yu KK, Hricak H. Imaging prostate cancer. *Radiology Clin. North Am.* 2000;38:59-85.
8. Folkman J. What is the evidence that tumors are angiogenesis dependent? *J. Natl. Cancer Inst.* 1990;82:4-6.
9. Konerding MA, Miodonski AJ, Lametschwandtnr A. Microvascular corrosion casting in the study of tumor vascularity: A review. *Scanning Microscopy*. 1995;9:1233-44.
10. Catalona WJ, Smith DS, Ratliff TL, Dodds KM, Coplen DE, Yuan JJ, Petros JA, Andriole GL. Measurements of prostate-specific antigen in serum as a screening test for prostate cancer. *N.Engl. J. Med.* 1991;324:1156-1161.
11. Catalona WJ, Richie JP, Ahmann FR, Hudson MA, Scardino PT, Flanigan RC, deKernion JB, Ratliff TL, Kavoussi LR, Dalkin BL. Comparison of digital rectal examination of prostate cancer: results of a multicenter clinical trial of 6,630 men. *Journal of Urology*. 1994;156:1283-1290.

12. Aarnink RG, Beerlage HP, Rosette JJDL, Dbruyne FM, Wijkstra H. Transrectal ultrasound of the prostate: innovations and future applications. *Journal of Urology*. 1998;159:1568-79.
13. Cooner WH, Mosley BR, Rutherford CLJ, Beard JH, Pond HS, Terry WJ, Igel TC, Kidd DD. Prostate cancer detection in a clinical urological practice by ultrasonography, digital rectal examination, and prostate specific antigen. *Journal of Urology*. 1990;143:1146-1152.
14. Djavan B, Zlotta A, Remzi M, Ghawidel K, Basharkhah A, Schulman CC, Marberger M. Optimal predictors of prostatic cancer on repeat prostate biopsy: a prospective study of 1,051 men. *Journal of Urology*. 2000;163:1144-1148.
15. Albertsen PC, Hanley JA, Harlan LC, Gilliland FD, Hamilton A, Liff JM, Stanford JL, Stephenson RA. The positive yield of imaging studies in the evaluation of men with newly diagnosed prostate cancer: a population based analysis. *Journal of Urology*. 2000;163:1138-1143.
16. Krouskop TA, Wheeler TM, Kallel F, Garra BS, Hall T. Elastic moduli of breast and prostate tissues under compression. *Ultrasonic Imaging*. 1998;20:260-274.
17. Skovoroda AR, Klishko AN, Gukasyan DA, Maevskiy EI, Ermilova VD, Oranskaya GA, Sarvazyan AP. Quantitative analysis of the mechanical characteristics of pathologically changed soft biological tissues. *Biophysics, Pergamon*. 1995;40:1359-1364.
18. Khaled W, Neumann T, Stapf J, Ermert H. PVA prostate phantom for ultrasound and MR elastography. *Proceedings of the Fourth International Conference on the Ultrasonic Measurement and Imaging of Tissue Elasticity*. 2005:105.
19. Fromageau J, Brusseau E, Vray D, Gimenez G, Delachartre P. Characterization of the PVA Cryogel. *IEEE Transactions on Ultrasonics, Ferroelectrics, and Frequency Control*. 2003;50:1318-1324.
20. Chu K, B.K.Rutt. Polyvinyl Alcohol Cryogel: An ideal phantom material for MR studies of arterial flow and elasticity. *Magnetic Resonance in Medicine*. 1997;37:314-319.
21. Beck J, Sethuraman S, Mallidi S, Karpiouk A, Aglyamov SR, Emelianov SY. Tissue mimicking materials and phantoms for elasticity imaging. *Proceedings of the Fourth International Conference on the Ultrasonic Measurement and Imaging of Tissue Elasticity*. 2005:107.
22. Emelianov SYY, Skovoroda AR, Lubinski MA, Shapo BM, O'Donnell M. Ultrasound elasticity imaging using Fourier based speckle tracking algorithm. In: *Proceedings of the 1992 IEEE Ultrasonics Symposium*; 1992:1065-68.
23. O'Donnell M, Emelianov SY, Skovoroda AR, Lubinski MA, Weitzel WF, Wiggins RC. Quantitative Elasticity Imaging. In: *IEEE Ultrasonic Symposium Proceedings*; 1993:893-903.
24. Chen X, Zohdy MJ, Emelianov SY, O'Donnell M. Lateral speckle tracking using synthetic lateral phase. *IEEE Transactions on Ultrasonics, Ferroelectrics, and Frequency Control*. 2004;51:540-550.
25. Lubinski MA, Emelianov SY, O'Donnell M. Adaptive strain estimation using retrospective processing. *IEEE Transactions in Ultrasonics, Ferroelectrics, and Frequency Control*. 1999;46:97-107.
26. Emelianov SY, Erkamp RQ, Lubinski MA, Skovoroda AR, O'Donnell M. Non-linear tissue elasticity: Adaptive elasticity imaging for large deformations. In: *Proceedings of the 1998 IEEE Ultrasonics Symposium*; 1998:1753-56.
27. Emelianov SY, Lubinski MA, Skovoroda AR, Erkamp RQ, Leavey SF, Wiggins RC, O'Donnell M. Reconstructive ultrasound elasticity imaging for renal pathology detection. In: *Proceedings of the 1997 IEEE Ultrasonics Symposium*; 1997.

28. Skovoroda AR, Lubinski MA, Emelianov SY, O'Donnell M. Reconstructive elasticity imaging for large deformations,. *IEEE Transactions in Ultrasonics, Ferroelectrics, and Frequency Control*,. 1999;46:523-535.
29. Skovoroda AR, Emelianov SY, Lubinski MA, Sarvazyan AP, O'Donnell M. Theoretical analysis and verification of ultrasound displacement and strain imaging,. *IEEE Transactions on Ultrasonics, Ferroelectrics, and Frequency Control*. 1994;41:302-313.
30. Skovoroda AR, Emelianov SY, O'Donnell M. Reconstruction of tissue elasticity based on ultrasound displacement and strain images. *IEEE Transactions in Ultrasonics, Ferroelectrics, and Frequency Control*,. 1995;42:747-765.
31. Lubinski MA, Emelianov SY, Raghavan KR, Yagle AE, Skovoroda AR, O'Donnell M. Lateral displacement estimation using tissue incompressibility. *IEEE Transactions on Ultrasonics, Ferroelectrics, and Frequency Control*. 1996;43.
32. Lubinski MA, Emelianov SY, O'Donnell M. Cross-correlation speckle tracking techniques for ultrasound elasticity imaging. *IEEE Transactions in Ultrasonics, Ferroelectrics, and Frequency Control*,. 1999;46:82-96.
33. Emelianov SY, Lubinski MA, Skovoroda AR, Erkamp RQ, Leavey SF, Wiggins RC, O'Donnell M. Reconstructive ultrasound elasticity imaging for renal transplant diagnosis: kidney ex-vivo results. *Ultrasonic Imaging*. 2000;22:178-194.
34. Ophir J, Cespedes I, Garra B, Ponnekanti H, Huang Y, Maklad N. Elastography: ultrasonic imaging of tissue strain and elastic modulus in vivo. *European Journal of Ultrasound*. 1996;3:49-70.
35. Sarvazyan AP, Skovoroda AP, Emelianov SY, Fowlkes JB, Pipe JG, Adler RS, Buxton RB, Carson PL. Biophysical bases of elasticity imaging,. In: Jones JP, ed. *Acoustical Imaging 21*. New York: Plenum Press; 1995:223-240.
36. Cohn NA, Emelianov SY, Lubinski MA, O'Donnell M. An elasticity microscope. Part I: Methods. *IEEE Transactions on Ultrasonics, Ferroelectrics, and Frequency Control*. 1997;44:1304-1319.

APPENDICES:

None